Comparison of ab Initio and DFT Methods for Studying Chain Propagation and Chain Termination Processes with Group 4 Polymerization Catalysts. 1. The *ansa*-Bis(cyclopentadienyl)zirconium Catalyst

Giovanni Talarico,*[,†] Arno N. J. Blok,[‡] Tom K. Woo,[§] and Luigi Cavallo*[,||]

Dipartimento di Chimica, Università di Napoli, Complesso Monte S. Angelo, I-80126 Napoli, Italy, Department of Inorganic Chemistry, University of Nijmegen, Toernooiveld 1, 6525 ED Nijmegen, The Netherlands, Department of Chemistry, University of Western Ontario, London N6A 5B7, Ontario, Canada, and Dipartimento di Chimica, Università di Salerno, Via Salvador Allende, I-84081 Baronissi (SA), Italy

Received April 22, 2002

In this paper we present a systematic comparison of the performance of different computational approaches to study the propagation and termination reactions of olefins with a prototype homogeneous group 4 *ansa*-metallocene catalyst. Chain propagation, β-H transfer to the monomer, and β-H elimination to the metal have been investigated for the $H_2Si(Cp)_2ZrR^+$ (R = ethyl, *n*-butyl) + C_2H_4 system using ab initio and density functional theory (DFT) techniques. For all the species investigated, all the computational approaches we considered result in substantially similar geometries. A comparison of the DFT and Møller−Plesset theory (MP2) propagation and termination barriers with extrapolated coupled-cluster calculations with inclusion of single, double, and perturbatively connected triple excitation (CCSD(T)) values indicates that all the pure functionals considered underestimate the difference between termination and propagation by roughly 3−4 kcal/mol. In contrast, hybrid functionals are within 1 kcal/mol from extrapolated CCSD(T) values. For a comparison with experimental results inclusion of zero-point energy contributions and the use of an alkyl group longer than ethyl to simulate the growing chain in both termination reactions are mandatory.

Introduction

Molecular weight and molecular weight distribution are among the most important properties of a polymer. Molecular weights must fit both performance and processability requirements, and this means molecular weights in the range 40 000−300 000. The molecular weight of a polyolefin (here defined as the average degree of polymerization, $\bar{P}_n$) made with single-site group 4 catalysts is given by eq 1, where R_P is the overall rate of propagation and the R_T values are the rates of all chain termination reactions.

$$\bar{P}_n = \frac{R_P}{\sum R_T} \quad (1)$$

Hence, understanding and modeling the detailed mechanisms of chain propagation and termination are the keys to molecular weight control.

The currently accepted mechanisms of chain propagation and termination for olefin polymerization with group 4 metallocene catalysts are summarized in Scheme 1.[1] The chain propagation (CP) mechanism, named after Cossee,[2−4] basically occurs in two steps: (i) olefin coordination to a vacant sit and (ii) migration of the σ-bonded growing chain to the π-coordinated olefin. Green, Rooney, and Brookhart slightly modified this mechanism, introducing an α-agostic interaction which would facilitate the insertion reaction.[5,6] The two main chain termination reactions are (i) bimolecular β-hydrogen transfer (BHT) from the growing chain to a coordinated olefin molecule and (ii) unimolecular β-hydrogen elimination (BHE) from the growing chain to the metal.[7]

Theoretical calculations suggested that BHT starts with an olefin-coordinated species with the growing chain involved in a β-agostic interaction with the metal.[8]

* To whom correspondence should be addressed. E-mail: G.T., talarico@chemistry.unina.it; L.C., lcavallo@unisa.it.
† Università di Napoli.
‡ University of Nijmegen.
§ University of Western Ontario.
|| Università di Salerno.

(1) Of course, polymerization conditions such as temperature, monomer concentration, and catalyst/cocatalyst ratio strongly influence the molecular weights, but these aspects are out of the scope of the present paper.

(2) Breslow, D. S.; Newburg, N. R. *J. Am. Chem. Soc.* **1959**, *81*, 81.
(3) Cossee, P. *Tetrahedron Lett.* **1960**, *17*, 17.
(4) Cossee, P. *J. Catal.* **1964**, *3*, 80.
(5) Brookhart, M.; Green, M. L. H. *J. Organomet. Chem.* **1983**, *250*, 395.
(6) Laverty, D. T.; Rooney, J. J. *J. Chem. Soc., Faraday Trans. 1* **1983**, *79*, 869.
(7) Brintzinger, H. H.; Fischer, D.; Mülhaupt, R.; Rieger, B.; Waymouth, R. M. *Angew. Chem., Int. Ed. Engl.* **1995**, *34*, 1143.
(8) Lohrenz, J. C. W.; Woo, T. K.; Ziegler, T. *J. Am. Chem. Soc.* **1995**, *117*, 12793.

10.1021/om020315i CCC: $22.00
Publication on Web 10/15/2002

Scheme 1

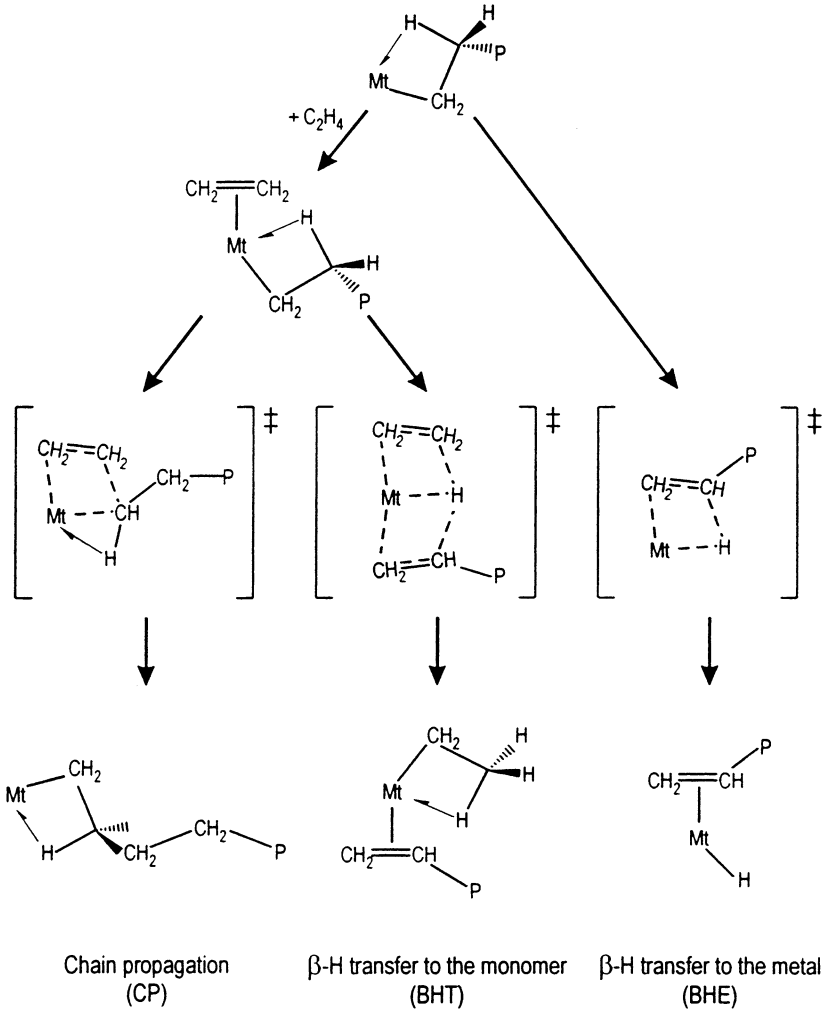

The β-agostic H atom shifts from the growing chain to the coordinated olefin, generating a vinyl-terminated growing chain and a new alkyl group σ-bonded to the metal. After dissociation of the long-chain olefin, coordination and insertion of a new monomer molecule into the Mt−alkyl bond starts the growth of a new polymer. BHT is thought to be the dominant chain transfer pathway in the polymerization of propene at heterogeneous catalysts[9−11] as well as at relatively unhindered *ansa*-zirconocenes.[7]

Instead, the BHE reaction starts from an olefin-free species with the growing chain involved in a β-agostic interaction with the metal. The product is a vinyl-terminated chain (as in the BHT reaction) and a metal hydride. After displacement of the long-chain olefin by a monomer, insertion into the Mt−H bond starts the growth of a new chain. Both neutral group 3 and cationic group 4 metallocene alkyl complexes were shown to be in equilibrium with hydride olefin complexes.[12−15]

Thus, the CP and BHT reactions share the initial alkyl olefin complex as a common intermediate (see Scheme 1), while the BHE reaction corresponds to a completely independent path.

Theoretical studies of olefin polymerization with density functional theory (DFT), Hartree−Fock (HF), second-order Møller−Plesset theory (MP2), and post-HF computational approaches contributed greatly to the understanding of both propagation and termination reactions. Nevertheless, the height of the CP barrier is still a matter of debate, since pure DFT approaches and some MP2 calculations predict the CP reaction to be almost barrierless,[8,16−20] whereas other MP2 and post-HF calculations predict a CP barrier in the range of 5−10 kcal/mol.[18,21−28]

(9) Zakharov, V. A.; Bukatov, G. D.; Yermakov, Y. I. *Adv. Polym. Sci.* **1983**, *51*, 61.
(10) Kashiwa, N.; Yoshitake, J. *Polym. Bull.* **1984**, *11*, 479.
(11) Pino, P.; Rotzinger, B.; von Achenbach, E. *Makromol. Chem.* **1985**, *25*, 461.
(12) Burger, B. J.; Thompson, M. E.; Cotter, W. D.; Bercaw, J. E. *J. Am. Chem. Soc.* **1990**, *112*, 1566.
(13) Hajela, S.; Bercaw, J. E. *Organometallics* **1994**, *13*, 1147.
(14) Alelyunas, Y. W.; Guo, Z.; LaPointe, R. E.; Jordan, R. F. *Organometallics* **1993**, *12*, 544.
(15) Guo, Z.; Swenson, D.; Jordan, R. *Organometallics* **1994**, *13*, 1424.
(16) Lauher, J. W.; Hoffmann, R. *J. Am. Chem. Soc.* **1976**, *98*, 1729.
(17) Weiss, H.; Ehrig, M.; Ahlrichs, R. *J. Am. Chem. Soc.* **1994**, *116*, 4919.
(18) Jensen, V. R.; Børve, K. J. *J. Comput. Chem.* **1998**, *19*, 947.
(19) Woo, T. K.; Fan, L.; Ziegler, T. *Organometallics* **1994**, *13*, 2252.
(20) Meier, R. J.; van Doremaele, G. H. J.; Iarlori, S.; Buda, F. *J. Am. Chem. Soc.* **1994**, *116*, 4.
(21) Kawamura-Kuribayashi, H.; Koga, N.; Morokuma, K. *J. Am. Chem. Soc.* **1992**, *114*, 8687.
(22) Castonguay, L. A.; Rappé, A. K. *J. Am. Chem. Soc.* **1992**, *114*, 5832.
(23) Axe, F. U.; Coffin, J. M. *J. Phys. Chem.* **1994**, *98*, 2567.
(24) Yoshida, T.; Koga, N.; Morokuma, K. *Organometallics* **1995**, *14*, 746.

With regard to the termination reactions, BHT from an ethyl group to a coordinated ethene molecule was predicted to have a barrier of about 10 kcal/mol.[8,26,29] BHE from an ethyl group was calculated to be much more difficult than BHT, with a barrier of about 20 kcal/mol.[19,24,26,29,30] Here, changing to a longer alkyl chain reduced the barrier to about 10−15 kcal/mol.[24,26,30]

Computer modeling of this class of reactions is becoming a useful tool in the exploration for new catalysts. Such usage requires an accurate calibration of the methodology employed. In this respect, comparative studies of the CP reaction with different methodological approaches were performed by Jensen and Børve, who investigated ethene insertion into $Cl_2TiCH_3^+$ and showed that DFT approaches are well-suited to study the CP reaction.[18] These and other authors stressed that first-row transition-metal complexes are more difficult to treat at the MP2 level than complexes of second- and third-row metals because of the presence of near-degeneracy effects due to the compactness of 3d orbitals.[31]

More recently, Lanza, Fragalà, and Marks investigated ethene insertion into the $Cp_2MCH_3^+$ and $H_2Si(Cp)(^tBuN)MCH_3^+$ systems (M = Ti, Zr) using HF and MP2.[28] They showed that geometry optimization at the HF level followed by single-point MP2 calculations represents a reasonable approach to investigate the CP reaction. However, the MP2 geometries were found to be somewhat different from the HF geometries.

The above studies offered interesting mechanistic insights but were limited to the CP reaction with the growing chain replaced by a simple methyl group. Moreover, Jensen and Børve replaced the real Cp ligands with Cl atoms, while Lanza, Fragalà, and Marks only compared HF and MP2 approaches and did not consider DFT, which is becoming the standard choice in the study of organometallic reactions with medium-sized systems (30−50 atoms or more). To our knowledge, a systematic comparison of the performances of different methodologies (both ab initio and DFT based) for "real" systems is still missing. More importantly, such studies (even with simplified systems) are totally missing for termination reactions promoted by group 4 polymerization catalysts, although similar studies on ethene polymerization promoted by Al systems evidenced remarkable discrepancies between DFT and ab initio results.[32,33]

Thus, it is not clear to what extent the available computational tools can be used to make reasonable predictions of the molecular weights for new catalysts. To clarify this, we here present a systematic study of the CP, BHT, and BHE reactions of the prototype *ansa*-metallocene system $H_2Si(Cp)_2ZrR^+$ (R = ethyl, *n*-butyl), which entails the core of many catalysts used for ethene and stereospecific 1-olefin homopolymerization, as well as for their copolymerization. We examined this system with various pure and hybrid DFT approaches and with classical ab initio HF and MP2 techniques. The effects of the basis set size on the activation barriers was evaluated at the DFT and MP2 levels. A comparison with coupled cluster calculations with inclusion of single, double, and perturbatively connected triple excitations results (CCSD(T)), which can be considered the most accurate for systems of this size, is also presented.

It is generally accepted that the ethyl group is long enough to represent the growing chain in the CP reaction with minimal energetic and/or geometric approximations.[26] For the BHT reaction, an alkyl group longer than ethyl has minimal effects on the geometries and small effects on the energetics of the reaction (the barrier is usually 1−2 kcal/mol lower).[34,35] In view of the number of methodologies considered, we decided to model the growing chain with an ethyl group also for the BHT reaction, but some test calculations on the CP and BHT reactions with the growing chain modeled by a *n*-butyl group will also be discussed. Finally, the use of an ethyl group to model the growing chain in the BHE reaction was shown to be inappropriate;[26] therefore, we used a *n*-butyl group here. In the present work we confine ourselves to the ethene insertion and chain transfer reactions promoted by a second-row *ansa*-metallocene catalyst. In a subsequent paper we will treat the merits of DFT versus ab initio methods for first- and second-row *ansa*-cyclopentadienyl−amido catalysts.[36]

Computational Details

Stationary points on the potential energy surface were calculated with the Gaussian98[37] and Gamess-UK[38] packages. Minima were localized by full optimization of the starting structures, while the transition states for the insertion reaction were approached through a linear transit procedure starting from the olefin-coordinated intermediate and then located by a full transition state search. The following quantum-mechanics methods were used. For wave function based methods, we used Hartree−Fock (HF) and second-order Møller−Plesset theory (MP2).[39] For the DFT calculations the following func-

(25) Jolly, C. A.; Marynick, D. S. *J. Am. Chem. Soc.* **1989**, *111*, 7968.
(26) Thorshaug, K.; Støvneng, J. A.; Rytter, E.; Ystenes, M. *Macromolecules* **1998**, *31*, 7149.
(27) Petitjean, L.; Pattou, D.; Ruiz-López, M. F. *J. Phys. Chem. B* **1999**, *103*, 27.
(28) Lanza, G.; Fragalà, I. L.; Marks, T. J. *Organometallics* **2001**, *20*, 4006.
(29) Cavallo, L.; Guerra, G. *Macromolecules* **1996**, *29*, 2729.
(30) Prosenc, M.-H.; Brintzinger, H.-H. *Organometallics* **1997**, *16*, 3889.
(31) Niu, S.; Hall, M. B. *Chem. Rev.* **2000**, *100*, 353−405.
(32) Talarico, G.; Budzelaar, P. H. M.; Gal, A. W. *J. Comput. Chem.* **2000**, *21*, 398.
(33) Talarico, G.; Barone, V.; Budzelaar, P. H. M.; Adamo, C. *J. Phys. Chem. A* **2001**, *105*, 9014.
(34) Cavallo, L.; Guerra, G.; Corradini, P. *J. Am. Chem. Soc.* **1998**, *120*, 2428.
(35) Talarico, G.; Budzelaar, P. H. M.; Barone, V.; Adamo, C. *Chem. Phys. Lett.* **2000**, *329*, 99.
(36) Talarico, G.; Blok, A.; Budzelaar, P. H. M.; Cavallo, L. Manuscript in preparation.
(37) Frisch, M. J.; Trucks, G. W.; Schlegel, H. B.; Scuseria, G. E.; Robb, M. A.; Cheeseman, J. R.; Zakrzewski, V. G.; Montgomery, J. A., Jr.; Stratmann, R. E.; Burant, J. C.; Dapprich, S.; Millam, J. M.; Daniels, A. D.; Kudin, K. N.; Strain, M. C.; Farkas, O.; Tomasi, J.; Barone, V.; Cossi, M.; Cammi, R.; Mennucci, B.; Pomelli, C.; Adamo, C.; Clifford, S.; Ochterski, J.; Petersson, G. A.; Ayala, P. Y.; Cui, Q.; Morokuma, K.; Malick, D. K.; Rabuck, A. D.; Raghavachari, K.; Foresman, J. B.; Cioslowski, J.; Ortiz, J. V.; Stefanov, B. B.; Liu, G.; Liashenko, A.; Piskorz, P.; Komaromi, I.; Gomperts, R.; Martin, R. L.; Fox, D. J.; Keith, T.; Al-Laham, M. A.; Peng, C. Y.; Nanayakkara, A.; Gonzalez, C.; Challacombe, M.; Gill, P. M. W.; Johnson, B. G.; Chen, W.; Wong, M. W.; Andres, J. L.; Head-Gordon, M.; Replogle, E. S.; Pople, J. A. *Gaussian 98*, revision A.9; Gaussian, Inc.: Pittsburgh, PA, 1998.
(38) Guest, M. F.; Fantucci, P.; Harrison, R. J. Kendrick, J.; van Lenthe, J. H.; Schoeffel, K.; Sharwood, P. GAMESS-UK (6.3) Generalised Atomic and Molecular Electronic Structure System; Daresbury Laboratory, Warrington, U.K.

Table 1. Geometries of the Olefin-Free $H_2Si(Cp)_2ZrC_2H_5^+$ Species[a]

	B3LYP	BP86	PBE	BPW91	BLYP	B1LYP	HF	MP2
				Distances (Å)				
$Zr-X_{Cp1}$	2.175	−0.012	−0.031	−0.014	+0.017	+0.003	+0.024	−0.013
Zr−C1	2.229	+0.010	−0.015	+0.009	+0.021	−0.001	−0.003	+0.013
Zr−H21	2.127	−0.023	−0.024	−0.019	+0.007	+0.005	+0.063	+0.023
C1−C2	1.504	−0.005	−0.009	−0.006	+0.005	+0.002	+0.015	+0.013
C2−H21	1.168	+0.017	+0.001	+0.013	+0.011	−0.003	−0.023	−0.019
C2−H22	1.099	+0.008	−0.001	+0.006	+0.006	−0.001	−0.012	−0.001
				Angles (deg)				
$X_{Cp1}-Zr-X_{Cp2}$	129.5	+0.6	+0.9	+0.7	−0.2	−0.2	−0.9	+0.3
θ	4.3	−2.5	−0.4	−3.1	+2.3	+0.9	+12.6	+57.4
Zr−C1−C2	85.5	−0.6	−0.6	−0.6	+0.1	+0.1	+1.3	−0.8
C1−C2−H21	113.2	+0.1	+0.6	+0.2	−0.3	+0.0	+0.2	+1.6
Zr−C1−H11	114.8	−1.0	−0.1	−1.0	−0.8	+0.2	+2.0	+2.1

[a] Atom numbering and the angle θ are defined in Figure 1. X_{Cp} is the centroid of the Cp ring.

tionals were used: (1) BP86, which corresponds to Becke's[40] exchange and Perdew's 1986[41,42] correlation functionals; (2) PBE, which is generated from the exchange-correlation functional of Perdew, Burke, and Ernzerhof;[43] (3) BPW91, which corresponds to Becke's[40] exchange and to Perdew and Wang's 1991 correlation functionals;[44,45] (4) BLYP, which corresponds to Becke's[40] exchange and to Lee, Yang, and Parr's correlation functional;[46] (5) B3LYP, which corresponds to Becke's three-parameter hybrid exchange[47] and to the Lee, Yang, and Parr's correlation functionals;[46] (6) B1LYP, which corresponds to Becke's one-parameter hybrid exchange[48] and to the Lee, Yang, and Parr's correlation functional[46] as implemented by Adamo and Barone.[49] Single-point CCSD(T) calculations[50,51] were performed on the B3LYP geometries. The Gaussian98 package was used for all the DFT, HF, and MP2 calculations, while the single-point CCSD(T) calculations were performed with Gamess-UK.

With the exception of the MP2 geometries, the real nature of all these structures as minima or as first-order saddle points was verified by frequency calculations, which resulted in none or only one imaginary frequency, respectively.

The all-electron MIDI basis set of Huzinaga was used for the Zr atom;[52] for all other atoms we used the split-valence + polarization basis set (p on H, pure d functions on C and Si) of Ahlrichs, denoted as SVP[53] (polarization functions were also included on all the atoms of the $H_2Si(Cp)_2$ ligand). For the single-point CCSD(T) calculations we had to use a smaller basis set: ECP LANL2DZ on Zr,[54−56] 6-31G(d,p)[57−61] (*p* on H, Cartesian *d* functions on C) on the H and C atoms of the ethene and of the alkyl group which simulates the growing chain, and 6-31G for the H, C, and Si atoms of the $H_2Si(Cp)_2$ ligand. Where not explicitly stated, the MP2 and CCSD(T) calculations were performed with the frozen-core approximation, excluding the 1s orbital on C, up to 2p on Si, and up to 3d on Zr.

Finally, to investigate the effect of the basis set we performed MP2 and B3LYP single-point calculations with the following basis sets: (1) LANL2DZ on Zr, 6-31G on all other atoms; (2) LANL2DZ on Zr, 6-31G on H_2SiCp_2, 6-31G(d,p) on the remaining atoms; (3) LANL2DZ on Zr, 6-31G on H_2SiCp_2, 6-311G(d,p) on the remaining atoms; (4) MIDI on Zr with the outermost two s orbitals and one p and d orbital split off and one f polarization function ($\alpha_f = 0.8$), SVP on all other atoms, or alternatively 6-31G(d,p) on H_2SiCp_2 and 6-311G(d,p) on the remaining atoms. To investigate the effects of the basis set (both at the MP2 and B3LYP level), we decided to use the B3LYP geometries for the following reasons: (i) while geometry optimizations at the B3LYP level are the routine for systems of this size, it is difficult to imagine that MP2 will be used as the standard approach in the investigation of these systems; (ii) using the same set of geometries for both the B3LYP and MP2 single-point calculations allows for a direct comparison of the effect of the basis set on the results obtained with the two computational approaches.

Results and Discussion

Olefin-Free Zr Alkyls. For the sake of readability, we use the B3LYP geometries as reference structures throughout this paper; geometrical values from the other theoretical approaches are reported as deviations from the B3LYP values. The most important geometrical parameters of the olefin-free $H_2Si(Cp)_2ZrC_2H_5^+$ species are reported in Table 1 with the atom numbering given in Figure 1.

All geometries are roughly C_s symmetric, since the C1−C2 and C2−H21 bonds lie in the equatorial belt of the metallocene. All geometries are also characterized by the presence of a rather strong β-agostic interaction, since the Zr−H21 distances are in the range 2.10−2.15 Å, with the exception of the HF geometry. The pure BP86, PBE, and BPW91 functionals result in a stronger agostic interaction (shortest Zr−H21 distances), while the HF approach gives the rather longer value of 2.19 Å.

Distances predicted by all methods are rather similar: the average absolute deviation from the B3LYP distances in Table 1 is only 0.013 Å. For the angles the average absolute deviation is 2.8° if the large deviation of the MP2 θ angle (see below) is also included and only 1.2° if it is not.

(39) Møller, C.; Plesset, M. S. *Phys. Rev.* **1934**, *46*, 618.
(40) Becke, A. *Phys. Rev. A* **1988**, *38*, 3098.
(41) Perdew, J. P. *Phys. Rev. B* **1986**, *33*, 8822.
(42) Perdew, J. P. *Phys. Rev. B* **1986**, *34*, 7406.
(43) Perdew, J. P.; Burke, K.; Ernzerhof, M. *Phys. Rev. Lett.* **1996**, *77*, 3865.
(44) Perdew, J. P.; Burke, K.; Wang, Y. *Phys. Rev. B* **1996**, *54*, 16533.
(45) Perdew, J. P. In *Electronic Structure of Solids '91*; Ziesche, P., Eschrig, H., Eds.; Akademie Verlag: Berlin, 1991; p 11.
(46) Lee, C.; Yang, W.; Parr, R. G. *Phys. Rev. B* **1988**, *37*, 785.
(47) Becke, A. D. *J. Chem. Phys.* **1993**, *98*, 5648.
(48) Becke, A. D. *J. Chem. Phys.* **1996**, *104*, 1040.
(49) Adamo, C.; Barone, V. *Chem. Phys. Lett.* **1997**, *274*, 242.
(50) Raghavachari, K.; Trucks, G. W.; Pople, J. A.; Head-Gordon, M. *Chem. Phys. Lett.* **1989**, *157*, 479.
(51) Purvis, G. D.; Bartlett, R. J. *J. Chem. Phys.* **1982**, *76*, 1910.
(52) Huzinaga, S.; Andzelm, J.; Klobukowsi, M.; Radzio-Andzelm, E.; Sakai, Y.; Tatewaki, H. *Gaussian Basis Sets for Molecular Calculations*; Elsevier: Amsterdam, 1984.
(53) Schaefer, A.; Horn, H.; Ahlrichs, R. *J. Chem. Phys.* **1992**, *97*, 2571.
(54) Hay, P. J.; Wadt, W. R. *J. Chem. Phys.* **1985**, *82*, 270.
(55) Hay, P. J.; Wadt, W. R. *J. Chem. Phys.* **1985**, *82*, 284.
(56) Hay, P. J.; Wadt, W. R. *J. Chem. Phys.* **1985**, *82*, 299.
(57) Ditchfield, R.; Hehre, W. J.; Pople, J. A. *J. Chem. Phys.* **1971**, *54*, 724.
(58) Hehre, W.; Ditchfield, J. R.; Pople, J. A. *J. Chem. Phys.* **1972**, *56*, 2257.
(59) Hariharan, P. C.; Pople, J. A. *Mol. Phys.* **1974**, *27*, 209.
(60) Gordon, M. S. *Chem. Phys. Lett.* **1980**, *76*, 163.
(61) Hariharan, P. C.; Pople, J. A. *Theo. Chim. Acta* **1973**, *28*, 213.

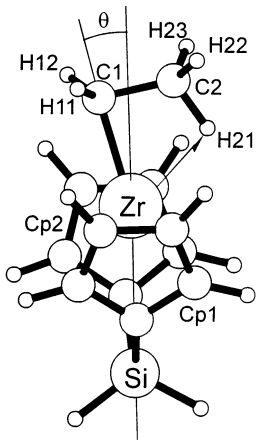

Figure 1. Minimum-energy geometry of $H_2Si(Cp)_2ZrC_2H_5^+$.

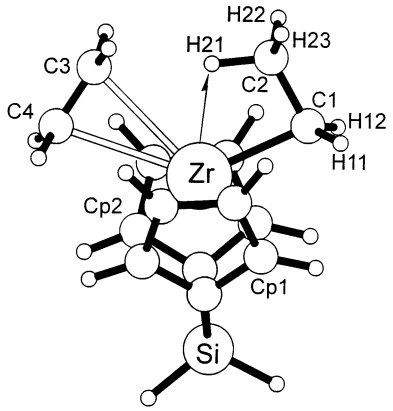

Figure 2. Minimum-energy geometry of $H_2Si(Cp)_2ZrC_2H_5$-$(C_2H_4)^+$.

HF and all the DFT methods predict that the Zr−C bond almost lies on the local symmetry axis, which is coincident with the Si−Zr axis. In contrast, the MP2 structure has the Zr−C bond bent away from this axis by over 60°. This result is consistent with earlier MP2 calculations on $H_2Si(Cp)_2ZrCH_3^+$, which also produced a rather large θ angle.[28,62]

The optimal position of the Zr−C σ-bond in naked (prior to olefin coordination) group 4 polymerization catalysts is a topic which was discussed extensively,[17,18,21−23,28,62,63] and a consensus has not been reached yet. However, all authors agree that whatever geometry is preferred (on or off the Si−Zr axis) the swing motion of the Zr−C σ-bond in the equatorial belt is easy. To check for the flatness of the potential energy surface relative to the swing motion of the Zr−C bond, we performed a geometry optimization at the B3LYP level with the angle θ fixed at the MP2 value of 61.7°. The optimized structure is only 0.8 kcal/mol higher in energy than the unconstrained B3LYP geometry. However, in catalytic systems of industrial interest, with ligands bulkier than the simple H_2SiCp_2 model used here and with a growing chain bulkier than the simple C_2H_5 group, steric interactions may be important in determining the best geometry.

Olefin Complexes. As for the olefin-free species, the overall structure of $H_2Si(Cp)_2ZrC_2H_5(C_2H_4)^+$ is substantially C_s symmetric, since the C−C bonds of both the olefin and of the C_2H_5 group are in the equatorial belt of the metallocene. The geometry of the olefin-bound intermediate is depicted in Figure 2 with the geometric details reported in Table 2.

For the olefin π complex the greatest geometric differences between the computational approaches are in the metal−olefin distances. While the B*n*LYP functionals result in Zr−C(ethene) distances close to 2.9 Å, the BP86, BPW91, PBE, and MP2 distances are roughly 0.1 Å shorter. On the other hand, HF predicts distances that are longer by 0.2 Å. In all cases the olefin can be considered symmetrically coordinated, since the two Zr−C(ethene) distances differ on average by only 0.012 Å; the BP86 geometry presents the largest difference (0.031 Å). Apart from these differences, the overall geometries are rather similar; the average absolute deviations from the B3LYP values in Table 2 are only 0.040 Å for distances and 0.7° for angles.

With regard to the energetics of ethene coordination, all DFT ethene uptake energies are in the relatively small range of 13−19 kcal/mol; the higher values correspond to the pure functionals. The MP2 uptake energy is much higher (25.8 kcal/mol), while the HF uptake energy is by far the lowest (7.0 kcal/mol only). The CCSD(T) value (21.5 kcal/mol) is intermediate between MP2 and DFT results. Zero-point energy (ZPE) corrections lower all uptake energies by roughly 3 kcal/mol. To check for the effect of the geometry on the uptake energy, we performed MP2//B3LYP single-point calculations. The value obtained, 24.8 kcal/mol, is only 1 kcal/mol lower than the original MP2 value, demonstrating the softness of the Zr−olefin interaction. Clearly, the differences in uptake energies are not due to geometrical differences.

For B3LYP, HF, and MP2 we also evaluated the influence of the basis set superposition error (BSSE) on the uptake energy, using the counterpoise correction of Boys and Bernardi.[63] BSSE is rather large at the MP2 level (12.9 kcal/mol) and smaller for CCSD(T) (8.6 kcal/mol), B3LYP (7.0 kcal/mol), and HF (4.9 kcal/mol). The HF BSSE was found to increase to 7.4 kcal/mol at the MP2 geometry. Thus, BSSE does change with the geometry, but it more strongly depends on the level of theory. Correction for BSSE reduces the MP2, B3LYP, and HF uptake energies from 25.9, 14.1, and 7.0 kcal/mol to 13.0, 7.1, and 2.1 kcal/mol, respectively. Thus, after correction the difference between the B3LYP and MP2 uptake energies is reduced from 11.8 to 5.9 kcal/mol. Improving the basis set at the MP2 level, MIDI + 1f on Zr and 6-311G(d,p) on the remaining atoms, leaves the coordination energy substantially unchanged, 25.3 kcal/mol, while the BSSE is reduced to 7.1 kcal/mol. These results indicate that BSSE corrections must be considered for gas-phase calculations of olefin uptake energies, particularly at the MP2 level.

CP Transition State. We were not able to locate the Cossee four-center transition state for the insertion of ethene in $H_2Si(Cp)_2ZrC_2H_5^+$ with the pure BP86, PBE, and BPW91 functionals. With the B*n*LYP functionals (either pure or hybrid) as well as at the HF and MP2 levels of theory we found this transition state, and the

(62) Cavallo, L. In *Computational Modelling of Homogeneous Catalysis*; Maseras, F., Lledos, A., Eds.; Kluwer Academic Publishers: Dordrecht, The Netherlands, in press.

(63) Bierwagen, E. P.; Bercaw, J. E.; Goddard, W. A., III. *J. Am. Chem. Soc.* **1994**, *116*, 1481.

Table 2. Geometries and Ethene Uptake Energies for the Olefin-Bound $H_2Si(Cp)_2ZrC_2H_5(C_2H_4)^+$ Species[a]

	B3LYP	BP86	PBE	BPW91	BLYP	B1LYP	HF	MP2
				Distances (Å)				
$Zr-X_{Cp1}$	2.195	−0.011	−0.033	−0.013	+0.019	+0.004	+0.022	−0.021
Zr−C1	2.295	+0.033	−0.009	+0.030	+0.033	−0.004	−0.040	+0.016
Zr−C3	2.921	−0.084	−0.078	−0.071	+0.005	+0.013	+0.232	−0.115
Zr−C4	2.925	−0.119	−0.088	−0.102	+0.002	+0.014	+0.252	−0.117
Zr−H21	2.167	−0.043	−0.038	−0.037	+0.007	+0.009	+0.087	−0.048
Zr−H22	3.384	−0.016	−0.037	−0.016	+0.023	+0.004	+0.042	−0.034
C1−C2	1.500	−0.007	−0.011	−0.007	+0.006	+0.002	+0.015	−0.005
C2−H21	1.147	+0.021	+0.004	+0.017	+0.011	−0.003	−0.021	+0.000
C3−C4	1.348	+0.015	+0.001	+0.014	+0.012	−0.002	−0.018	+0.008
C3−H21	2.254	−0.128	−0.087	−0.115	−0.009	+0.017	+0.191	−0.053
				Angles (deg)				
$X_{Cp1}-Zr-X_{Cp2}$	127.5	+0.3	+0.6	+0.4	−0.1	+0.0	−0.3	+0.2
Si−Zr−C1	111.3	−0.9	−1.1	−0.9	+0.3	+0.2	+3.7	−2.7
Si−Zr−C4	112.5	+1.0	+0.5	+1.1	+0.1	+0.0	−1.0	+0.2
C1−Zr−C4	136.1	+0.0	+0.7	−0.2	−0.4	+0.0	−2.7	+2.5
Zr−C1−C2	85.8	−1.7	−1.0	−1.5	−0.4	+0.2	+2.9	−1.8
Zr−C4−C3	76.5	+0.8	+0.0	+0.7	+0.0	+0.1	+0.4	−0.6
C1−C2−H21	113.1	+0.4	+0.5	+0.5	+0.1	+0.0	−0.3	+0.5
Zr−C2−H11	115.8	−0.5	+0.2	−0.4	−0.3	+0.2	+1.1	+0.3
				Ethene Binding Energy (kcal/mol)				
E(binding)	14.1 (11.3)	16.8 (13.9)	18.7 (16.0)	14.6 (11.6)	13.3 (10.4)	13.5 (10.7)	7.0 (4.6)	25.9

[a] Atom numbering is defined in Figure 2. X_{Cp} is the centroid of the Cp ring. Uptake energies in parentheses include ZPE corrections.

vibrational analysis always produced one imaginary frequency corresponding to the expected transition vector. In the case of the BP86 functional we investigated this aspect in further detail. To this end we performed a linear transit by varying the length of the emerging C−C bond in the range 2.60−2.20 Å with steps of 0.025 Å. This resulted in a rather flat downhill path: all these structures are within 0.8 kcal/mol, with no signs of a transition state. Our findings are consistent with the BP86 study of the $C_2H_4 + Cp_2ZrC_2H_5^+$ insertion reaction by Ziegler and co-workers.[8] They also found a flat and downhill path, with a transition state of negligible barrier (0.8 kcal/mol) at a C−C distance of 2.30 Å. According to them, the highest transition state between the olefin-bound β-agostic intermediate (as in Figure 2) and the γ-agostic insertion product does not correspond to the Cossee four-center transition state but to the rupture of the β-agostic interaction and the rotation of the chain out of the equatorial belt of the metallocene.

Recent studies on ethene insertion reactions in the presence of a counterion (usually $CH_3B(C_6F_5)_3^-$, μ-CH_3 coordinated to the metal) showed that the insertion barrier is definitely higher than in the absence of the counterion (close to 10 kcal/mol), even with the BP86 functional.[65] For this reason, we decided to approximate the BP86, PBE, and BPW91 CP transition states through constrained-geometry optimizations with the emerging C−C bond fixed at 2.230 Å, which is the value it assumes in the B3LYP transition state. Thus, the BP86, PBE, and BPW91 "transition state" geometries and insertion barriers of Table 3 correspond to these constrained-geometry optimizations. The atom numbering is given in Figure 3.

The various B*n*LYP functionals give almost identical structures, with the forming C−C bond close to 2.23 Å. The MP2 CP transition state is slightly more reactant-like, since the emerging C−C and Zr−C(ethene) bonds are 0.05 Å longer, while the breaking $Zr-C(C_2H_5)$ bond is 0.03 Å shorter. Whatever approach is used, all the structures of Table 3 are characterized by the usual α-agostic interaction with Zr−H11 distances close to 2.07 Å, with the exception of the larger HF value of 2.13 Å.

Excluding the HF value, the CP barriers (calculated as the energy difference between the transition states of Table 3 and the corresponding olefin-bound intermediates of Table 2) are in the relatively narrow range of 2.8−6.4 kcal/mol. The lowest values correspond to the pure functionals, while for the other approaches higher barriers result from higher amounts of HF exchange in the functional. The MP2 insertion barrier is slightly higher than all the DFT barriers. The HF insertion barrier is definitely the highest, 11.4 kcal/mol, a feature already observed by other authors.[31] Inclusion of ZPE contributions slightly increases the CP insertion barrier (by roughly 0.2 kcal/mol).

To check for the influence of the length of the alkyl group used to simulate the growing chain on the height of the CP barrier, we performed B3LYP and BLYP calculations using a *n*-butyl group. This substitution does not change the geometries of Table 3 much and results in CP barriers of 4.9 and 4.3 kcal/mol, respectively, which are identical with those obtained for insertion into the shorter ethyl group.

BHT Transition State. At the HF level, we were unable to locate a true BHT transition state. Instead, the reaction appears to start with β-H elimination, followed by associative displacement of the olefin by a second ethene molecule via a hydride bis(olefin) complex (Figure 4). This complex is of rather higher energy (25.7 kcal/mol relative to the olefin-coordinated species of Table 2); both olefin molecules are weakly coordinated to the metal, as indicated by the rather long ethene coordination distances. To facilitate comparison with the other methods, we approximated the HF "transition state" by fixing the C2−H and C3−H distances at the B3LYP value of 1.485 Å.

With all the other methodologies we located an approximately C_{2v} symmetric BHT transition state. The

(64) Boys, S. F.; Bernardi, F. *Mol. Phys.* **1970**, *19*, 553.
(65) Chan, M. S. W.; Ziegler, T. *Organometallics* **2000**, *19*, 5182.

Table 3. Geometries of the Transition State and Energy Barriers for the CP Reaction in C_2H_4 + $H_2Si(Cp)_2ZrC_2H_5^+$ [a]

	B3LYP	BP86	PBE	BPW91	BLYP	B1LYP	HF	MP2
				Distances (Å)				
$Zr-X_{Cp1}$	2.203	−0.012	−0.033	−0.014	+0.020	+0.003	+0.024	−0.024
$Zr-X_{Cp2}$	2.199	−0.014	−0.035	−0.015	+0.019	+0.004	+0.025	−0.021
Zr−C1	2.289	+0.004	−0.017	+0.007	+0.033	+0.005	+0.035	−0.032
Zr−C4	2.391	−0.006	−0.020	−0.009	+0.000	−0.003	−0.023	+0.046
Zr−C3	2.627	−0.015	−0.029	−0.017	+0.007	+0.002	+0.030	−0.011
Zr−H11	2.068	−0.016	−0.016	−0.015	+0.005	+0.004	+0.064	−0.022
C1−C3	2.230	fixed	fixed	fixed	−0.023	−0.009	−0.036	+0.052
C1−H11	1.151	+0.014	+0.002	+0.010	+0.009	−0.002	−0.020	+0.003
C1−H12	1.098	+0.008	+0.002	+0.008	+0.007	−0.001	−0.010	+0.001
C1−C2	1.513	+0.001	−0.010	+0.000	+0.009	+0.001	+0.004	−0.005
C3−C4	1.406	+0.011	−0.003	+0.010	+0.016	+0.000	+0.000	−0.013
				Angles (deg)				
$X_{Cp1}-Zr-X_{Cp2}$	127.5	+0.6	+0.9	+0.6	−0.1	+0.0	−0.7	+1.1
Si−Zr−C1	157.1	+0.8	+0.7	+0.8	+0.3	−0.1	−2.3	+1.2
Si−Zr−C4	117.7	−1.4	−1.6	−1.4	+0.5	+0.5	+4.2	−2.7
Zr−C1−C2	141.1	+0.2	−0.7	+0.8	+0.9	+0.0	+0.4	−0.8
Zr−C1−H11	64.3	−1.0	−0.1	−1.1	−1.2	+0.0	+1.8	+0.2
Zr−C1−H12	107.9	−0.5	+0.4	−0.9	−1.0	+0.0	+0.3	−0.1
Zr−C1−C3	71.1	−0.6	−0.6	−0.7	+0.0	+0.1	+0.9	−0.7
Zr−C4−C3	83.2	−0.6	−0.4	−0.6	+0.0	+0.2	+2.3	−2.0
C1−Zr−C4	85.1	+0.7	+1.0	+0.7	−0.7	−0.3	−1.8	+1.6
				Chain Propagation Barrier (kcal/mol)				
E	4.8 (5.1)	2.8	3.4	2.8	4.3 (4.3)	5.2 (5.5)	11.4 (12.3)	6.4

[a] Atom numbering is defined in Figure 3. X_{Cp} is the centroid of the Cp ring. Energy barriers in parentheses include ZPE corrections. For the BP86, PBE, and BPW91 "transition states", geometry and energy were obtained through a constrained minimization with the emerging C−C bond fixed at 2.23 Å. For these cases, no ZPE-corrected values are reported.

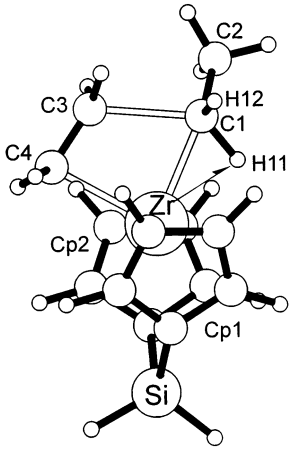

Figure 3. Transition state for ethene insertion into the Zr−C σ-bond of $H_2Si(Cp)_2ZrC_2H_5^+$.

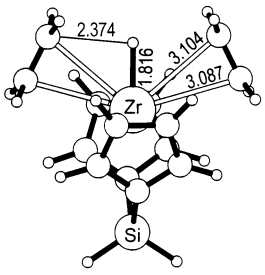

Figure 4. Minimum-energy geometry of the HF bis(olefin) species.

BHT transition state geometries are reported in Table 4, with the atom numbering given in Figure 5. Independent of the computational approach, the emerging and breaking C−H bonds are in the narrow range of 1.45−1.50 Å.

The DFT and MP2 BHT activation barriers (calculated as the energy difference between the transition states of Table 4 and the corresponding olefin-bound intermediates of Table 2) vary between 6.7 and 13.3 kcal/mol. The lowest values correspond to the pure BP86 and BPW91 functionals. In this case, the MP2 barrier is lower than that of the two hybrid B3LYP and B1LYP functionals and rather similar to the PBE and BLYP values. The HF barrier is much higher (30.6 kcal/mol). Finally, it is noteworthy that all the BHT barriers, in contrast to the CP ones, are lowered by roughly 2 kcal/mol by the inclusion of ZPE corrections.

As we did with the CP barrier, also for the BHT we checked for the influence of the length of the alkyl group used to simulate the growing chain, using an *n*-butyl group at the BP86, BLYP, and B3LYP levels. This substitution does not change the geometries of Table 4 much, but it breaks the near-C_{2v} symmetry of the transition state; the H−C(ethene) distance of 1.50 Å is now 0.02 Å longer than the H−C(*n*-butyl) distance. The presence of the longer alkyl group reduces the BHT barrier, calculated relative to $H_2Si(Cp)_2Zr(n\text{-butyl})(C_2H_4)^+$, by roughly 1.5 kcal/mol at all the levels of theory.

BHE Transition State. This is the species where geometrical differences between different approaches are greatest but the barriers calculated are the most similar. Since previous studies showed that energetics and geometries of the BHE reaction depend strongly on the length of the alkyl group, we used a *n*-butyl group to model the growing chain.

The geometries of the BHE transition state are reported in Table 5 with the atom numbering given in Figure 6.

While the different computational approaches showed small differences in the length of the emerging Zr−H σ-bond, which is in the range of 1.79−1.85 Å, there was a greater deviation in the length of the breaking C−H bond, which ranges between 1.77 and 2.21 Å. The

Table 4. Geometries of the Transition State and Energy Barriers for the BHT Reaction in $H_2Si(Cp)_2ZrC_2H_5(C_2H_4)^+$ [a]

	B3LYP	BP86	PBE	BPW91	BLYP	B1LYP	HF	MP2
				Distances (Å)				
$Zr-X_{Cp1}$	2.205	−0.015	−0.036	−0.016	+0.019	+0.003	+0.027	−0.032
Zr−C1	2.491	−0.008	−0.032	−0.008	+0.021	+0.003	+0.007	−0.026
Zr−C2	2.652	−0.016	−0.039	−0.016	+0.020	+0.006	+0.024	−0.050
Zr−H	1.983	+0.016	−0.008	+0.018	+0.023	−0.002	−0.024	−0.009
C1−C2	1.404	+0.012	−0.002	+0.011	+0.012	−0.002	−0.014	+0.008
C2−H	1.485	−0.016	−0.023	−0.019	+0.004	+0.006	fixed	−0.036
				Angles (deg)				
$X_{Cp1}-Zr-X_{Cp2}$	127.0	+0.5	+0.9	+0.5	−0.2	+0.0	−0.6	+1.4
Si−Zr−C1	114.9	−0.3	−0.5	−0.2	+0.2	+0.1	+1.2	−0.6
C1−Zr−C4	130.2	+0.7	+0.9	+0.5	−0.3	−0.1	−2.3	+1.2
Zr−C1−C2	80.6	−0.6	−0.5	−0.6	−0.1	+0.2	+1.0	−1.4
C1−C2−H	115.5	+1.3	+1.0	+1.3	+0.4	−0.2	−2.1	+1.8
C2−H−C3	162.5	+1.9	+1.8	+1.9	+0.2	−0.3	−4.6	+2.0
				Barrier of β-H Transfer to the Monomer, BHT, Reaction (kcal/mol)				
E	12.1 (10.3)	6.7 (4.7)	9.6 (7.6)	6.9 (4.9)	9.6 (7.5)	13.3 (11.5)	30.6	9.5

[a] Atom numbering is defined in Figure 5. X_{Cp} is the centroid of the Cp ring. Energy barriers in parentheses include ZPE corrections. For the HF "transition state", geometry and energy were obtained through a constrained minimization with the forming and breaking C−H bonds fixed at 1.485 Å. For this case, no ZPE-corrected value is reported.

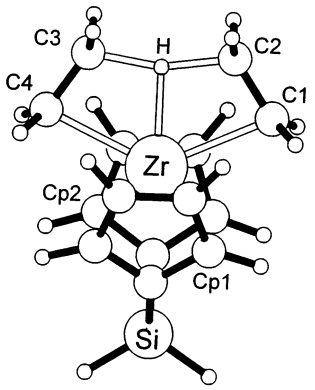

Figure 5. Transition state for the bimolecular β-hydrogen transfer to the monomer (BHT) termination reaction.

largest distances are predicted by the pure BP86, PBE, and BPW91 functionals, while the HF geometry is at the bottom end of the range. The MP2 BHE transition state is rather similar to the B3LYP geometry. The breaking Zr−C σ-bond is roughly 2.42 Å long, independent of the methodology, and it is only 0.1 Å longer than in the starting Zr−(*n*-butyl) species.

Although the geometries for the BHE transition state differ significantly among the methods examined, the activation barrier for this process is the most similar, HF included. All the barriers are in the range of 9.7−14.6 kcal/mol, with the BLYP and HF values at the bottom and top ends, respectively. Also for this termination reaction, inclusion of the ZPE corrections lowers the barrier (by ca. 2.5 kcal/mol).

Basis Set Effects. The difference between the BHT and BHE termination barriers with the CP barrier can be used to estimate the performance of the different methodological approaches in predicting molecular weights. For this, we need estimated "best" values for all the barriers. The effect of correlation was evaluated through CCSD(T) calculations. Due to the size of the system, these had to be performed with a smaller basis set, and thus, the CCSD(T) calculations are probably not converged. The effect of basis set extension was estimated with several single-point calculations at the MP2 and B3LYP level, up to considering a basis set with f functions at Zr, 6-31G(d,p) at the ligand, and 6-311G(d,p) at the reactive groups. These calculations are summarized in Table 6; combination of the correlation and basis set effects gives the "our best" values reported there.

At the MP2 level, inclusion of polarization functions on the 6-31G basis set of the C and H atoms of the reactive groups ($C_2H_5^-$ and C_2H_4) reduces the CP barrier considerably (compare entries 1 and 2), while it has a smaller effect on the BHT and BHE barriers. Extension of the basis set to 6-311G(d,p) on the reactive groups (compare entries 2 and 3) lowers all the activation barriers, the BHT in particular. Using the all-electron MIDI basis set on Zr and the SVP basis set on the remaining atoms results in lower CP and BHT barriers than with the 6-31G(d,p) basis of roughly the same size (compare entries 2 and 4); these values are closer to the ones obtained with the larger 6-311G(d,p) basis set of entry 3.

The increased flexibility in the Zr basis set of entry 6 scarcely lowers the CP and BHT barriers, while the BHE barrier remains unchanged. The extension of the active-orbital space (compare entries 4 and 5) to include all the occupied orbitals reduces the CP and BHT barriers only. Finally, the best MP2 values we obtained (entry 7) do not differ substantially from the values of entries 4−6, which suggests that improving further the quality of the basis set would not change the conclusions significantly.

At the MP2 level is it clear that the basis set influences the competition of both BHT and BHE with the CP reaction. However, we remark that the comparison of BHT and CP is straightforward because the two bimolecular processes share the initial olefin-coordinated species and, hence, will show similar dependencies on reaction conditions (solvent, temperature, monomer concentration). Their balance sets, in the framework depicted in Scheme 1, an *upper limit* on the molecular weight. To compare the unimolecular BHE and the bimolecular CP reactions, the coordination energy has to be added to the calculated BHE activation barrier, to obtain the same reference point. It makes this situation more complicated due to relevant influence of the entropic factors. Therefore, we will use the $\Delta E^{\ddagger}_{BHT-CP}$

Table 5. Geometries of the Transition State and Energy Barriers for the BHE Reaction in $H_2Si(Cp)_2Zr(n\text{-butyl})^+$ [a]

	B3LYP	BP86	PBE	BPW91	BLYP	B1LYP	HF	MP2
				Distances (Å)				
$Zr-X_{Cp1}$	2.178	−0.019	−0.041	−0.020	+0.018	+0.004	+0.027	−0.020
$Zr-X_{Cp2}$	2.183	−0.016	−0.041	−0.018	+0.017	+0.003	+0.024	−0.023
Zr−C1	2.414	+0.027	+0.038	+0.028	+0.006	−0.001	−0.003	+0.027
Zr−C2	2.745	+0.060	+0.040	+0.057	+0.015	−0.002	−0.004	−0.025
Zr−H21	1.824	−0.010	−0.023	−0.010	+0.020	+0.002	+0.024	−0.030
C1−C2	1.387	−0.006	−0.022	−0.006	+0.011	+0.000	+0.005	−0.009
C2−C3	1.502	−0.002	−0.012	−0.003	+0.010	+0.001	+0.002	−0.003
C2−H21	1.904	+0.307	+0.351	+0.274	+0.004	−0.023	−0.135	+0.033
				Angles (deg)				
$X_{Cp1}-Zr-X_{Cp2}$	128.9	+0.5	−0.1	+0.6	−0.2	−0.1	−0.8	−0.2
Si−Zr−C1	176.9	−2.8	−27.0	−3.3	+0.2	+0.9	−17.6	−13.4
Zr−C1−C2	88.2	+1.9	+0.8	+1.7	+0.2	−0.1	−0.2	−2.1
C1−C2−H21	102.7	−2.7	−2.1	−2.4	−0.1	+0.1	+0.5	+1.6
C1−C2−C3	124.5	+0.6	+0.4	+0.7	+0.0	−0.2	−0.9	−0.6
C1−C2−H21	102.7	−2.7	−2.1	−2.4	−0.1	+0.1	+0.5	+1.6
				Barrier for β-H Transfer to the Metal (kcal/mol)				
E	11.3 (8.9)	10.6 (8.3)	14.1 (11.5)	11.0 (8.7)	9.7 (7.3)	11.5 (9.0)	14.6 (11.7)	14.1

[a] Atom numbering is defined in Figure 6. X_{Cp} is the centroid of the Cp ring. Energy barriers in parentheses include ZPE corrections.

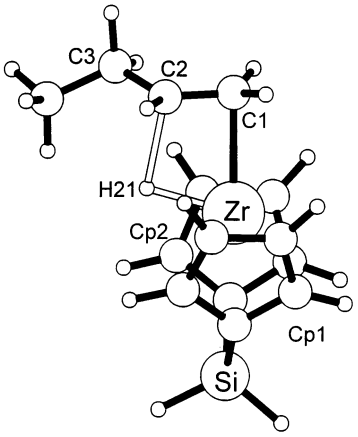

Figure 6. Transition state for the unimolecular β-hydrogen transfer to the metal (BHE) termination reaction.

values in Table 6 for the comparison with experimental data, whereas $\Delta E^{\ddagger}_{BHE-CP}$ is only indicative of the computational performance of the various methods but cannot be directly related to experiments.

While $\Delta E^{\ddagger}_{BHT-CP}$ is substantially independent of the basis sets, since it is in the range of 2.7−4.5 kcal/mol, $\Delta E^{\ddagger}_{BHE-CP}$ strongly depends on the basis set, since it increases from 0.4 kcal/mol for entry 1 to 9.6 kcal/mol for entry 7. This indicates that, at the MP2 level, basis sets of high quality are required. Improvement of the correlation treatment from MP2 to CCSD(T) (entries 2 and 8) has a large effect on $\Delta E^{\ddagger}_{BHT-CP}$. The extrapolated "our best" values (entry 9) show a much larger preference for propagation than the initial MP2 results of entries 1−7. These "our best" barriers will be used for a calibration of the different theoretical approaches used throughout this paper (Tables 3−5) and re-collected in the bottom half of Table 6, for the clarity of reading.

The effect of the basis set on the B3LYP values is definitely smaller than that on the MP2 values. In fact, the B3LYP barriers vary by less than 2 kcal/mol, whatever basis set or reaction is considered. This low sensitivity of the barriers to the basis set is also reflected in the more relevant $\Delta E^{\ddagger}_{BHT-CP}$ and $\Delta E^{\ddagger}_{BHE-CP}$ values, which vary by less than 1 and 3.5 kcal/mol, respectively.

Comparison between Theoretical Approaches. With regard to the absolute activation barriers, the pure BP86, PBE, and BPW91 functionals underestimate the CP barrier by roughly 3−4 kcal/mol. The B*n*LYP functionals perform better but still underestimate the "our best" barrier, although for B1LYP the difference is only 1.2 kcal/mol. The MP2 barrier slightly underestimated "our best" barrier, while the HF barrier is far too high; the MP2//HF CP barrier is much lower than the MP2//MP2 barrier. The situation for the BHT reaction is rather different. In this case the pure DFT functionals, the BLYP included, and the MP2 approach underestimate the "our best" value by roughly 5−7 kcal/mol. In contrast, the B3LYP and B1LYP hybrid functionals produce BHT barriers close to the "our best" value, while the HF barrier is again far too high. As for the CP reaction, MP2//HF underestimates the "our best" value. Finally, for the BHE reaction all the barriers are relatively close to each other, with both pure and hybrid DFT (with the exception of the PBE functional) slightly underestimating the "our best" value and the HF and MP2 values slightly overestimating it. With regard to the relative activation barriers $\Delta E^{\ddagger}_{BHT-CP}$ and $\Delta E^{\ddagger}_{BHE-CP}$, which represent the main goal of the present paper, all the pure DFT functionals and the MP2 approach underestimate the "our best" $\Delta E^{\ddagger}_{BHT-CP}$ value by 3−5 kcal/mol. The hybrid B3LYP and B1LYP functionals are much more balanced, since they are within 1 kcal/mol from the "our best" $\Delta E^{\ddagger}_{BHT-CP}$ value. This means that the hybrid functionals approximate to a similar extent the CP and BHT CCSD(T) barriers, whereas the pure functionals and MP2 specifically underestimate the BHT CCSD(T) barrier. As a consequence, molecular weight predictions, which depend on the relative heights of the CP and BHT barriers, can be reasonably estimated with the hybrid B*n*LYP functionals but will be certainly underestimated if pure functionals or MP2 are used. In a comparison of $\Delta E^{\ddagger}_{BHT-CP}$ and $\Delta E^{\ddagger}_{BHE-CP}$, it is worthy of note that all the pure DFT and the MP2 approaches predict that $\Delta E^{\ddagger}_{BHT-CP}$ is *smaller* than $\Delta E^{\ddagger}_{BHE-CP}$, whereas the hybrid B*n*LYP functionals, CCSD(T), and "our best" values predict that $\Delta E^{\ddagger}_{BHT-CP}$ is roughly 1−2 kcal/mol *larger* than $\Delta E^{\ddagger}_{BHE-CP}$.

Table 6. Activation Barriers, in kcal/mol, for the CP, BHT, and BHE Reactions, Calculated at Different Levels[a]

entry no.	basis set (Zr; ligand; reactive groups)	method	$E^{\ddagger}_{CP}$[a]	$E^{\ddagger}_{BHT}$[b]	$E^{\ddagger}_{BHE}$[c]	$\Delta E^{\ddagger}_{BHT-CP}$	$\Delta E^{\ddagger}_{BHE-CP}$
1	LANL2DZ; 6-31G; 6-31G	MP2 (B3LYP)	9.7 (6.2)	12.5 (13.8)	10.1 (10.3)	2.7 (7.6)	0.4 (4.1)
2	LANL2DZ; 6-31G; 6-31G(d,p)	MP2 (B3LYP)	6.9 (5.4)	11.4 (13.4)	11.7 (10.2)	4.5 (8.0)	4.8 (4.8)
3	LANL2DZ; 6-31G; 6-311G(d,p)	MP2 (B3LYP)	4.9 (5.6)	8.9 (13.5)	10.4 (10.8)	4.0 (7.9)	5.5 (5.2)
4	MIDI; SVP; SVP	MP2 (B3LYP)	5.9 (4.8)	9.6 (12.1)	13.9 (11.3)	3.8 (7.3)	8.0 (6.5)
5	MIDI; SVP; SVP (Full MP2)	MP2	4.5	7.9	13.8	3.4	9.3
6[d]	MIDI′+f; SVP; SVP	MP2 (B3LYP)	4.9 (4.2)	8.8 (12.5)	14.1 (11.8)	3.9 (8.3)	9.2 (7.6)
7[d]	MIDI′+f; 6-31G(d,p); 6-311G(d,p)	MP2 (B3LYP)	4.7 (5.3)	8.4 (13.2)	14.3 (11.3)	3.8 (7.9)	9.6 (5.9)
8	LANL2DZ; 6-31G; 6-31G(d,p)	CCSD(T)	8.6	17.3	12.9	8.7	4.5
9[e]		"our best"	6.4	14.3	12.1	7.9	5.7
10	MIDI; SVP; SVP	BP86	2.8[f]	6.7	10.6	3.9	7.8
11	MIDI; SVP; SVP	PBE	3.4[f]	9.6	14.1	6.2	10.7
12	MIDI; SVP; SVP	BPW91	2.8[f]	6.9	11.0	4.1	8.2
13	MIDI; SVP; SVP	BLYP	4.3	9.6	9.7	5.3	5.4
14	MIDI; SVP; SVP	B3LYP	4.8	12.1	11.3	7.3	6.5
15	MIDI; SVP; SVP	B1LYP	5.2	13.3	11.5	8.1	6.3
16	MIDI; SVP; SVP	HF	11.4	30.6[g]	14.6	19.2	3.2
17	MIDI; SVP; SVP	MP2	6.4	9.5	14.1	3.1	7.7
18	MIDI; SVP; SVP	MP2//HF	2.9	7.2	15.2	4.3	15.9

[a] Entries 10−17 correspond to the barrier of Tables 3−5. Entry 18 corresponds to MP2 single-point calculations on the HF geometries. [b] Activation barriers relative to the $H_2Si(Cp)_2ZrC_2H_5(C_2H_4)^+$ species. [c] Activation barriers relative to the $H_2Si(Cp)_2Zr(n\text{-butyl})^+$ species. [d] MIDI on Zr with the outermost s, p, and d orbitals uncontracted and one f polarization function ($\alpha_f = 0.8$). [e] "Best values": $E^{\ddagger}_X$[CCSD(T)] − $E^{\ddagger}_X$(MP2) of entry 8 summed to $E^{\ddagger}_X$(MP2) of entry 7. [f] Geometry optimized with the emerging C−C bond fixed at 2.23 Å. [g] Geometry optimized with the emerging C−H bond fixed at 1.48 Å.

Tentative Comparison with Experimental Data. Up to this moment, the discussion has been limited to a comparison between different theoretical approaches. Here, we will try to compare the gas-phase calculations reported in Table 6 with the experimentally determined molecular weights.[66] To make this comparison, *we have to assume* that the counterion and solvent effects should affect similarly the propagation and termination reactions. We did not try to model the cocatalyst used experimentally,[67] methylalumoxane, due to its elusive structure.[68] Instead, solvent effects were examined with single-point calculations for the CP, BHT, and BHE reactions at the B3LYP level, including toluene and CH_2Cl_2 as solvents of relatively different polarity. The polarizable continuum PCM model[69] as implemented in the Gaussian98 package was used.[70] All the absolute activation energies are decreased by roughly 1 and 3 kcal/mol in toluene and CH_2Cl_2, respectively, but the relative differences between them are substantially unchanged.

Under these assumptions, it is clear that the "our best" estimate of the $\Delta E^{\ddagger}_{BHT-CP}$ value around 8 kcal/mol would result in a polyethylene with a molecular weight higher than the value found experimentally.[67] However, as previously remarked, there are a few factors which have to be taken into account for a proper evaluation of $\Delta E^{\ddagger}_{BHT-CP}$. (1) When an alkyl group longer than ethyl is considered, the test BLYP and B3LYP calculations we performed indicated that the $E^{\ddagger}_{BHT}$ barrier relative to the π complex is lowered by roughly 1.5 kcal/mol while the $E^{\ddagger}_{CP}$ value is substantially invariant. (2) The ZPE contribution increases by roughly 0.5 kcal/mol the $E^{\ddagger}_{CP}$ barrier and lowers by roughly 2 kcal/mol the $E^{\ddagger}_{BHT}$ barrier (see Tables 3 and 4). Thus, for a comparison with the experimental data the $\Delta E^{\ddagger}_{BHT-CP}$ values of Table 6 must be lowered by about 2−3 kcal/mol. When this correction is applied, the $\Delta E^{\ddagger}_{BHT-CP}$ values of the pure functionals and of MP2 are in the range of 1−2 kcal/mol, which implies that only oligomers should be obtained. The hybrid B3LYP and B1LYP functionals and the "our best" $\Delta E^{\ddagger}_{BHT-CP}$ values are in the range of 4−5 kcal/mol and thus would predict molecular weights of the correct magnitude. The HF values are always far off and should never be used for molecular weight prediction.

Conclusions

We have performed a systematic comparison of the performances of different computational approaches in the ethene insertion and chain transfer reactions at the prototypical zirconocene catalyst $H_2Si(Cp)_2ZrR^+$. The main conclusions can be summarized as follows.

(1) All approaches considered result in substantially similar geometries. Pure BP86, PBE, and BPW91 functionals and MP2 show stronger agostic interactions and usually result in short distances of olefin coordination.

(2) With the pure BP86, PBE, and BPW91 functionals, ethene insertion is virtually barrierless and classical Cossee-like four-center transition states cannot be located. At the HF level, β-H transfer to monomer does not occur; the reaction instead follows a two-step path involving β-elimination and associative olefin displacement from the hydride. In all other cases, the expected transition states could be located.

(3) A comparison of the DFT and MP2 propagation and termination barriers with "our best" calculations indicates that all the pure functionals, BLYP included, and MP2 underestimate the BHT barrier in particular.

(4) As a consequence, pure functionals and MP2 underestimate the difference between termination and propagation barriers by roughly 3−4 kcal/mol. The

(66) In the literature it is reported that, at high ethene concentration and at 50 °C, the bis(cyclopentadienyl)zirconium systems produce polyethylene of $M_n = 80\,000$.[67] This corresponds to around 2800 ethene insertions and a $\Delta E^{\ddagger}_{BHT-CP}$ value of ∼5 kcal/mol.

(67) Kaminsky, W. *Macromol. Chem. Phys.* **1996**, *197*, 3907.

(68) While the absolute propagation and termination barriers can be modified sensibly by the inclusion of the counterion, it is more reasonable that the relative energy differences, which determine the molecular weights, are less influenced.

(69) Tomasi, J.; Persico, M. *Chem. Rev.* **1994**, *94*, 2027.
(70) Cossi, M.; Barone, V.; Cammi, R.; Tomasi, J. *Chem. Phys. Lett.* **1996**, *255*, 327.

hybrid functionals are within 1 kcal/mol from "our best" values. This means that only hybrid functionals can give a correct estimate of the molecular weights produced by the *ansa*-zirconocene catalyst.

(5) Finally, for a correct comparison with experimental results inclusion of zero-point energy contributions and the use of an alkyl group longer than ethyl to model the growing chain in the β-H transfer termination reactions is mandatory.

Acknowledgment. We thank Dr. P. H. M. Budzelaar for helpful suggestions and discussions. G.T. and L.C. thank the MURST of Italy (Grant PRIN-2000) and Basell Polyolefins for financial support and the CIMCF of Università "Federico II" of Naples for technical support. T.K.W. and L.C. thank the Sharcnet Project at the University of Western Ontario for unlimited access to their computer facilities. We thank Dr. J. H. van Lenthe for a generous grant of computer time and technical assistance. Part of this work was sponsored by the Stichting Nationale Computerfaciliteiten (National Computing Facilities Foundation, NCF) for the use of supercomputer facilities, with financial support from the Nederlandse Organisatie voor Wetenschappelijk Onderzoek (Netherlands Organization for Scientific Research, NWO).

Supporting Information Available: Tables giving coordinates and energies of all the species considered. This material is available free of charge via the Internet at http://pubs.acs.org.

OM020315I